

Adsorptive removal of trace uranium ions from simulated wastewater with FeCl₃-modified attapulgite with sodium alginate beads

Aixia Zhou, Jinsheng Wang*, Yuanhui Lin, Xin Guan, Rui Zuo, Yanguo Teng

College of Water sciences, Beijing Normal University, Beijing, 100088, China, Tel. +86 13811500321, email: zhousaixia2010@sina.com (A. Zhou), wangjs@bnu.edu.cn (J. Wang), 1293325460@qq.com (Y. Lin), 746429572@qq.com (X. Guan), 12901305@qq.com (R. Zuo), teng1974@163.com (Y. Teng)

Received 24 April 2017; Accepted 25 November 2017

ABSTRACT

The attapulgite (ATP) is a good adsorbent of heavy metal ion due to its high surface area, low cost and environmental compatibility. But the natural ATP has limited adsorption capacity and selectivity. In this study, a cost-effective and ready-generated adsorbent, FeCl₃-modified attapulgite (Fe-ATP), was evaluated to remove uranium ions from simulated wastewater. After preparation, Fe-ATP was characterized by fourier transform infrared spectroscopy (FTIR), scanning electron microscope (SEM), energy dispersive X-ray spectroscopy (EDS), transmission electron microscopy (TEM) analysis. The impacts of pH, contact time, ionic strength, temperature and initial U(VI) concentration on the adsorption capacity of Fe-ATP beads were examined. The adsorption kinetics of U(VI) dominated by the pseudo-second order model, and the adsorption isotherms fitted the Freundlich isotherm. The adsorption mechanism involved chemisorption, surface complexation and ions exchange. These results indicate that Fe-ATP bead is a cheap and promising adsorbent for the U(VI) removal and holds potential to be used for radioactive wastewater treatment.

Keywords: Attapulgite (ATP); Sodium alginate; Adsorption; Uranium; Wastewater

1. Introduction

With the rapid development of nuclear industry, the production of radioactive waste could give rise to serious pollution in environment [1]. The radioactive water released into the natural environment could be hazardous to public health causing detrimental sickness, such as kidney damage, lung insufficiency, muscle cramp, liver damage and even death [2,3]. Therefore, the highly efficient removal of radionuclides from aqueous solutions has become an issue of great concern. The adsorption technology is regarded to be one of the most extensive and promising methods to remove radionuclides from aqueous solution, due to the low cost, simple design, easy operation, and high feasibility [4–7]. Many types of adsorbents have been demonstrated to have the capacity for U(VI) adsorption, however,

the adsorption capacities of these adsorbents are not sufficiently high or they are not cost-effective [8–12]. Therefore, more efficient and cost-effective adsorbents with a high adsorption capacity are highly needed for U(VI) removal from wastewater.

ATP is a kind of hydrated octahedral layered magnesium aluminum silicate mineral with exchangeable cations in its framework channels and reactive –OH groups on its surface. It is a type of natural fibrous silicate clay, consisting of two double chains of the pyroxene-type (SiO₃)²⁻ like amphibole (Si₄O₁₁)⁶⁻ running parallel to the fibre axis [14]. ATP with high ion exchange capacity and rich reserve in the world (up to 1.5 hundred million tons) has been widely used to manage environment in recent years [13–15]. In the last decade, ATP or modified ATP has been investigated as an adsorbent in the removal of organic contaminants, heavy metal ions and radionuclides from aqueous solutions by using batch and spectroscopy techniques [16–25].

*Corresponding author.

However, the limited adsorption capacity and easy coagulation still hinder the application of ATP in environmental cleanup. Sodium alginate (SA), as a bountiful renewable resource, has attracted the attention of scientific researchers to be prepared as adsorbent for the removal of U(VI). SA is preferred over other materials because of its biodegradability, hydrophilicity and abundance in nature [26–29]. It is expected that nanoscale composite of SA with ATP could improve the type and amount of hydrophilic groups, network structure and properties of super adsorbents. But few studies combined ATP with SA to adsorb U(VI) from solution.

Herein, the Fe-ATP, synthesized and granulated with SA, was used as adsorbent to remove U(VI) ions from wastewater. The influences of contact time, pH, ionic strength, temperature and initial U(VI) concentration on U(VI) ions adsorption were researched. The adsorption mechanism of U(VI) on Fe-ATP bead was discussed in detail. This work may lead to the development of cheap and efficient radionuclide adsorbents for the treatment of wastewater and other radionuclide wastewaters.

2. Materials and methods

2.1. Materials

ATP used in this study was obtained from XuyiCity, Jiangsu Province, China. The $\text{UO}_2(\text{NO}_3)_2 \cdot 6\text{H}_2\text{O}$ was purchased from Chushengwei Chemical Co. Ltd. (Wuchang, China). Uranium stock solution of 1 g L^{-1} was prepared by dissolving $\text{UO}_2(\text{NO}_3)_2 \cdot 6\text{H}_2\text{O}$ in deionized water. The FeCl_3 was purchased from Fuchen Chemical reagent Co. (Tianjin, China). The other reagents were all analytical grade and purchased from Sinopharm Chemical Reagent Co. Ltd. (Shanghai, China).

2.2 Synthesis of Fe-ATP beads

Original ATP was purified according to the previous method [30] and sieved to 200 British Standard Sieve (BSS) meshes. Then the purified ATP was mixed with 2 mol L^{-1} of FeCl_3 solution (prepared by the dilute hydrochloric acid) with the ratio ($V_{\text{FeCl}_3 \text{ solution}}(\text{mL})/W_{\text{ATP}}(\text{g})$) of 5:1 to exchange the interlayer cations of ATP with Fe^{3+} . The mixture reacted for 90 min by magnetic stirring (H01-1B, Shanghai Mei Yingpu Instrument Manufacturing Co., Ltd, Shanghai, China) and dispersed in an ultrasonic bath (KQ-250DB, Kun Shan Ultrasonic Instruments Co., Ltd, Kunshan, China) for 1 h at 308 K. The mixtures centrifuged at 3300 rpm for 15 min (Biofuge primo R, Thermo Sorvall, Shanghai, China). The precipitate was washed repeatedly to remove the water-soluble particles. The Fe-ATP was aged for 2 h at 353K and then dried, crushed, and sieved to the particle size of a 100-mesh screen. The Fe-ATP powder mixed with sodium alga acid, dropped in the calcium chloride solution at constant

velocity to form the beads. The beads dried 2 h under 383 K and stored in an airtight container until further use.

2.3 Batch experiments

The batch adsorption experiments were carried out by adding a fixed amount of Fe-ATP beads (0.06 g) to a series of 250-mL conical flasks filled with 100 mL U(VI) diluted solution ($0.5\text{--}10 \text{ mg L}^{-1}$). The conical flasks were then sealed and shaken at 200 rpm at 308 K for the required time. Samples were collected at a given time interval and immediately analyzed after filtered through $0.45 \mu\text{m}$ Millipore membrane to remove suspended particles. The concentration of U(VI) solution was measured by spectrophotometric method (WGJ-III, Daji photoelectric instrument co., LTD, Hangzhou, China) referred to the method of Xiang et al. [31]. The adsorption percentage (adsorption, %) and adsorption capacity (Q_t , mg g^{-1}) could be calculated from Eqs. (1) and (2), respectively.

$$Q_t = \frac{V \times (C_0 - C_t)}{m} \quad (1)$$

$$\text{Adsorption}(\%) = \frac{(C_0 - C_t)}{C_0} \times 100\% \quad (2)$$

where C_0 and C_t (mg L^{-1}) are the initial concentration and residual concentration of U(VI), respectively, the $m(\text{g})$ is the mass of the adsorbents, and $V(\text{L})$ is the volume of the adsorption system.

The initial concentration was set to 0.01, 0.05, 0.1, 0.5, 1.0, 5.0 or 10.0 mg L^{-1} , while the initial pH was set at 2, 3, 4, 5, 7, 9 or 11 to investigate the effects of these factors on the adsorption of Fe-ATP beads. The pH of solution was adjusted by NaOH and HNO_3 . All experiments were replicated three times.

2.4. Analytical methods

Raw ATP and Fe-ATP were characterized by SEM-EDS (Hitachi S-4800/EX-350, Suzhou, China) and TEM (Tecnai G2 20, FEI Company, Hillsboro, USA) to analyze the size and morphology of the adsorbents in this work. The surface functional groups were identified by FTIR (Nexus 670, Nicolet, USA). The structures of ATP and Fe-ATP were analyzed by XRD (X'Pert PRO MPD, PANalytical B. V., Netherlands).

3. Results and discussions

3.1. Characteristics of the adsorbents

SEM micrographs of raw ATP bead and Fe-ATP bead are shown in Fig. 1. The SEM images showed that there were no obvious differences on the surface between the ATP bead (not shown) and Fe-ATP bead. The surface of Fe-ATP bead performed irregularly concave-convex and there were

Table 1
The main oxide content of ATP(%)

SiO_2	Al_2O_3	Fe_2O_3	Na_2O	K_2O	CaO	MgO	MnO	TiO	Others
60.9	10.01	6.7	0.11	1.35	1.95	11.35	0.01	0.67	6.95

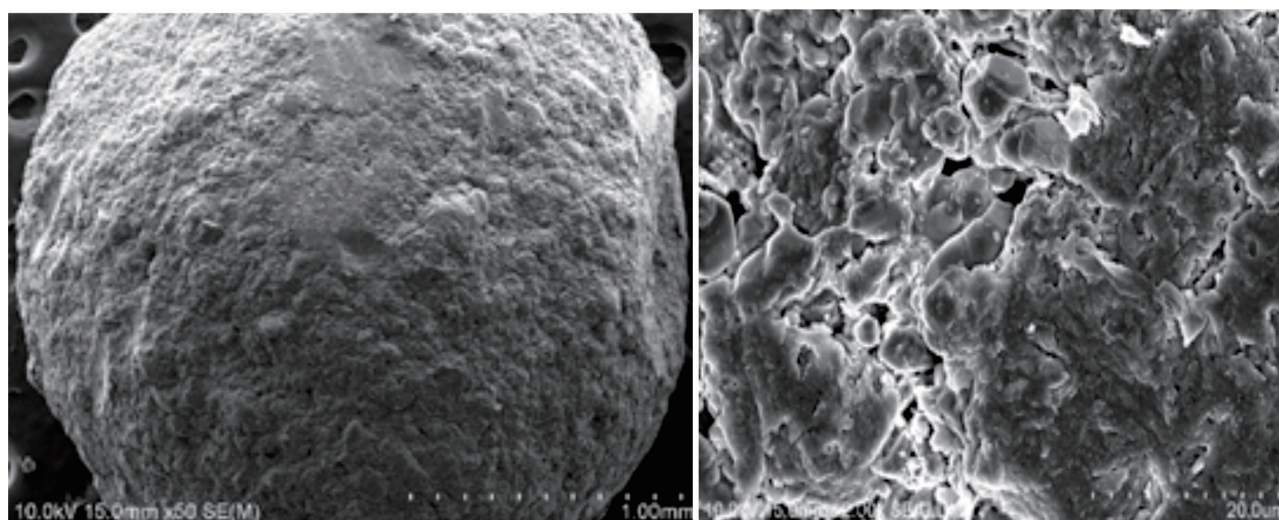


Fig. 1. SEM of the Fe-ATP bead.

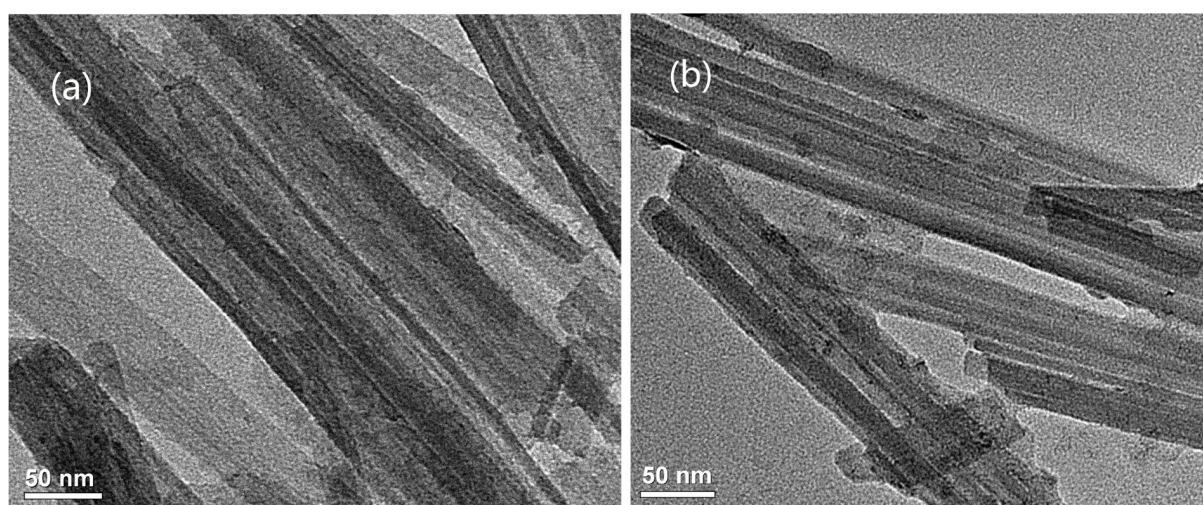


Fig. 2. TEM of the ATP(a) and Fe-ATP(b).

rather abundant of folds and pores to provide more chances for ionic sorption during the adsorption process.

In order to study the variation on structures of the ATP and Fe-ATP, TEM analysis was further employed in this research. Fig. 2 shows the TEM images of ATP and Fe-ATP. The nano-structures of ATP and Fe-ATP were observed. Some rods were densely overlapped and randomly oriented, and the morphology resembled rod fibres. It is clear that the loading of Fe^{3+} ions were on the surface of active sites of Fe-ATP.

The elemental compositions of the materials were obtained with EDS analysis, and the spectra are shown in Fig. 3. The results showed that C, Ca, Si, O, Mg, Al and K were the major elements of adsorbent beads. However, U uniquely presented in the EDS spectra of Fe-ATP after U(VI) adsorption, which indicated that the U(VI) ions had been adsorbed onto the Fe-ATP bead.

One important characteristic of adsorbent is the surface functional groups, which is largely characterized by the

FTIR spectroscopy method [32]. Fig. 4 shows the FTIR spectra of the ATP, Fe-ATP and Fe-ATP after U(VI) adsorption. The absorption bands appearing at 3405 cm^{-1} is attributed to the stretching of the O-H associated to zeolitic water of the clay mineral [33]. The band centered at 1637.46 cm^{-1} was assigned to the bending deformation of the zeolitic water molecules [34,42]. The band at 3553 cm^{-1} were attributed to the vibrations of hydroxyl groups M-OH (M = Al_2 , Al-Mg, Al- Fe^{3+} , Mg, Fe^{3+}) [36–42]. The peak at 1430 cm^{-1} was the characteristic peak of carbonate ion. The characteristic peak of Si-O was splitted into two peaks at 1031 cm^{-1} and 981 cm^{-1} respectively, which illustrated that there were two connection modes of Si-O in the ATP [43]. The band at 914 cm^{-1} was attributed to M-OH deformation [44]. The peaks at 510 cm^{-1} and 476 cm^{-1} were the specific adsorption peak of ATP. The band at 880 cm^{-1} was attributed to the vibrational mode of Al-Fe-OH [45]. These data were fundamental to confirm the ATP structure. Fig. 4 showed that after Fe-modified the characteristic peaks at 476 cm^{-1} disappeared. Due to

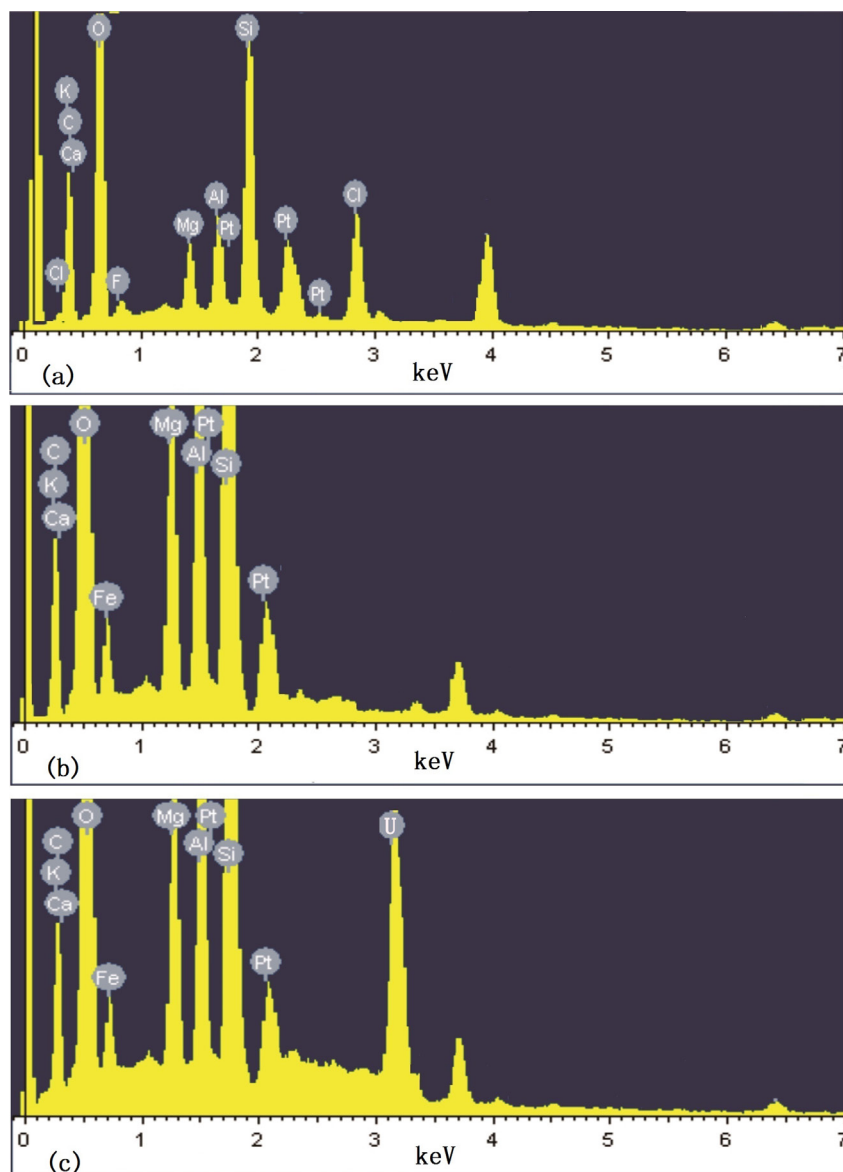


Fig. 3. EDS spectra of ATP bead (a), Fe-ATP bead (b) and after U (VI) adsorption (c).

the unity of Fe^{3+} and carbonate ion the peak at 1430 cm^{-1} disappeared or weakened. The peak at 903 cm^{-1} presented, which also belonged to the stretching vibration of uranyl ions [46].

As shown in Fig. 5, the XRD pattern of ATP changed weakly after it was modified by ferric chloride. The characteristic diffraction peaks of ATP were found, and the strong diffraction peaks at $2\theta = 8.49^\circ, 13.90^\circ, 19.85^\circ, 28.03^\circ$ and 35.32° could be ascribed to (110), (200), (040), (400) and (161) (PDF No. 00-021-0550) respectively, indicating the highly layer chain structure of ATP [46]. The peak (200) had the interplanar distance of $d = 6.30\text{ nm}$ which was attributed to the basal plane of ATP structure [47,48]. The intergrowth-minerals of montmorillonite (50.19°) and quartz (26.6°) was also found in the ATP. The peaks at $2\theta = 18.20^\circ, 39.06^\circ$ and 42.50° might be assigned to Fe-ATP composites.

3.2. Effect of contact time on U(VI) adsorption

The impacts of contact time on the U(VI) adsorption are depicted in Fig. 6. The initial U(VI) adsorption rate of Fe-ATP bead was more rapid compared to those of ATP bead, with more than 75% adsorption was achieved within 30 min. Such a rapid adsorption was probably attributed to the surface physical adsorption and chemical reactive adsorption as an immediate interaction between U(VI) ions and the reactive groups on the adsorbent surface [49]. With the adsorption sites approaching saturated, the U(VI) adsorption capacity of 8.19 mg g^{-1} was achieved after reaching adsorption equilibrium at 8.0 h.

3.3. Effect of pH and ionic strength on U(VI) adsorption

The pH of the aqueous solution is an important parameter for the adsorption of metal ions. It can affect the surface

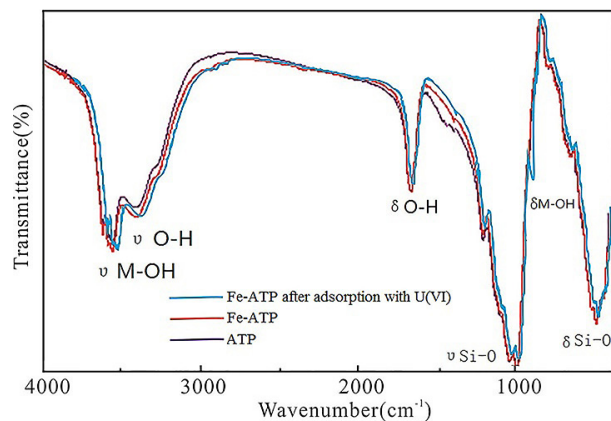


Fig. 4. FT-IR spectra for ATP and Fe-ATP before and after U(VI) adsorption.

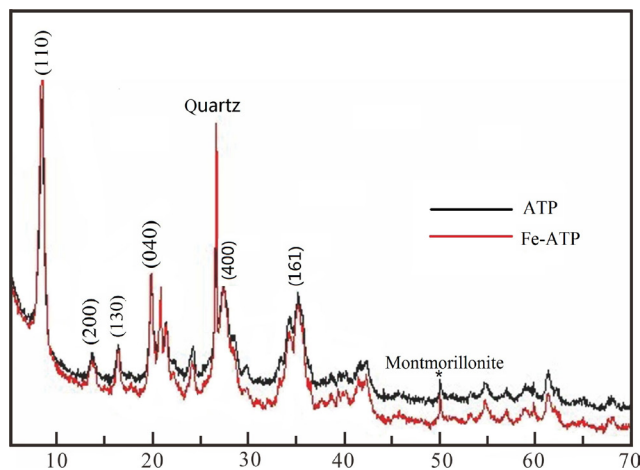


Fig. 5. The XRD patterns of ATP and Fe-ATP.

charge, the metal speciation and surface metal binding sites. The influences of pH on U(VI) adsorption by the adsorbent are illustrated in Fig. 7. The adsorption of U(VI) on ATP bead was strongly affected by pH and ionic strength. Adsorption of U(VI) increased quickly at pH 2–5, reached the maximum sorption at pH 6–7, and then decreased with increasing pH at pH > 7. The reason was that at lower pH value, the H^+ of solution would be rich and combined with $-NH_2$ to form $-NH_3^+$, which reduced the activity of adsorption site. So the competition between H_3O^+ and UO_2^{2+} limited the adsorption efficiency of U(VI) ions [50]. The $(UO_2)_3(OH)_7^-$ anions increased at pH > 8. These anions were known for their low sorption affinity and easily formed clathrate with CO_3^{2-} or HCO_3^- , so the amount of U(VI) adsorption decreased [51]. Therefore, the subsequent experiments was set at pH 5.5.

The influences of ionic strength on the U(VI) adsorption performance are shown in Fig. 8. The adsorption of U(VI) was the highest in 0.001 M NaCl solution, and the lowest in 0.5 M NaCl solution. These results suggested that ion exchange contributed to the adsorption of U(VI) by ATP bead and Fe-ATP bead from solution. The adsorption of U(VI) by ATP bead and Fe-ATP bead was mainly via ion exchange with hydrogen and sodium ions that saturated the exchange sites [52–54].

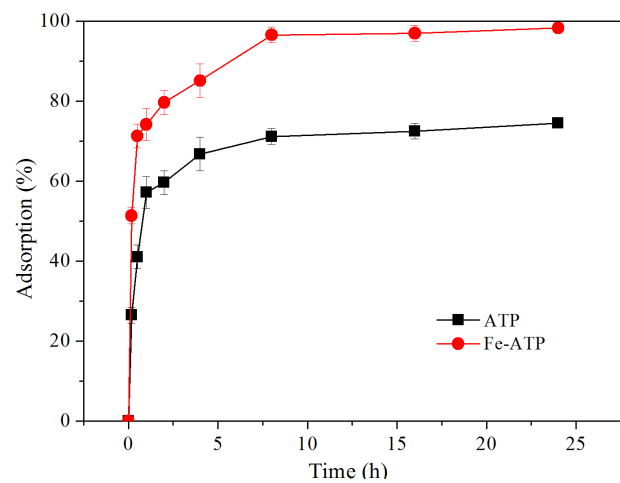


Fig. 6. The effect of contact time on adsorption of U(VI) on ATP bead and Fe-ATP bead (C_0 : 5 mg L^{-1} ; m : 0.06 g; T : 308K; 200 rpm).

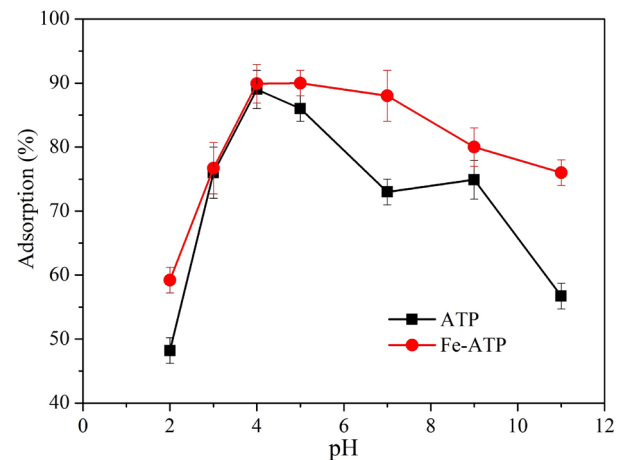


Fig. 7. The effect of pH on adsorption of U(VI) on ATP bead and Fe-ATP bead (C_0 : 5 mg L^{-1} ; m : 0.06 g; T : 308K; 200 rpm).

The pH and ionic strength affected the adsorption of U(VI) on ATP bead and Fe-ATP bead obviously, which suggested that the adsorption of U(VI) was dominated by surface complexation and ions exchange [55–57].

3.4. Effect of initial U(VI) concentration on U(VI) adsorption

The initial concentration provides an important driving force to overcome all mass transfer resistance of metal ions between the aqueous and solid phases [58]. Fig. 9 illustrated the influence of initial U(VI) concentration on the U(VI) adsorption. With increase of initial U(VI) concentration from 0.01 to 10.0 mg L^{-1} , the adsorption capacity of U(VI) on ATP bead and Fe-ATP bead increased rapidly. The sharp increase in adsorption capacity at a high U(VI) concentration was due to the increased concentration gradient at the solid-liquid interface [59]. Due to the depletion of active sites on the surface of ATP bead and Fe-ATP bead, the adsorption reached equilibrium.

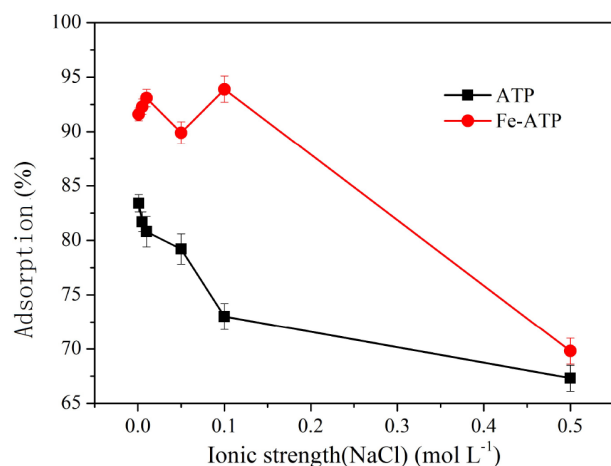


Fig. 8. The effect of ionic strength on adsorption of U(VI) on ATP bead and Fe-ATP bead (C_0 : 5 mg L⁻¹; m : 0.06 g; T: 308K; 200 rpm).

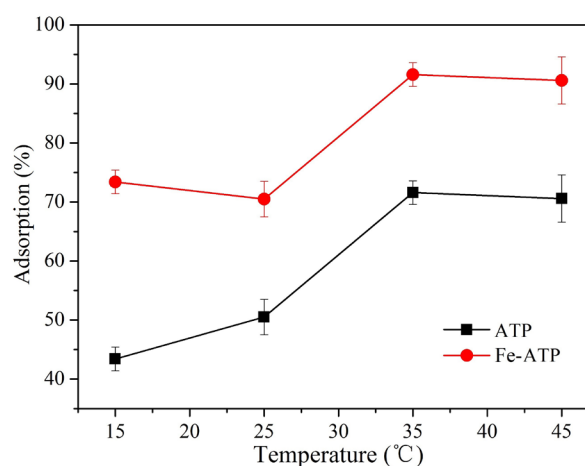


Fig. 10. The effect of temperature on adsorption of U(VI) on ATP bead and Fe-ATP bead (C_0 : 5 mg L⁻¹; m : 0.06 g; T: 308K; 200 rpm).

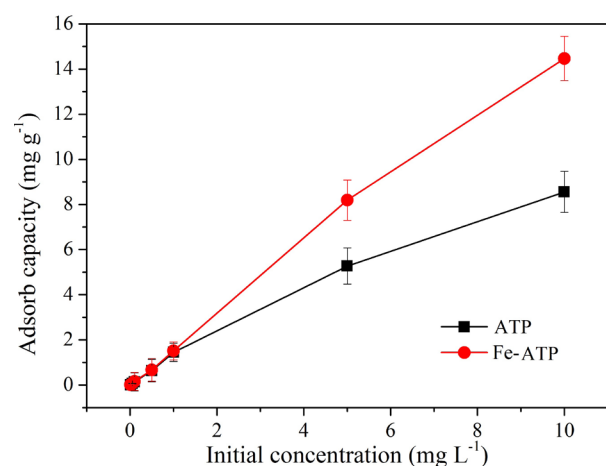


Fig. 9. The effect of Initial U(VI) concentration on adsorption of U(VI) on ATP bead and Fe-ATP bead (C_0 : 5 mg L⁻¹; m : 0.06 g; T: 308K; 200 rpm).

And the adsorption capacity of U(VI) on Fe-ATP bead was higher than that of U(VI) on ATP bead.

3.5. Effect of temperature on U(VI) adsorption

As seen from Fig. 10, the adsorption increased with the rise of temperature, indicating that the adsorption process of U(VI) on ATP bead and Fe-ATP bead was endothermic. According to the ambient temperature, the experimental temperature was controlled at around 308 K in all experiments (except this experiment). In comparison with the raw ATP bead and Fe-ATP bead, the Fe-ATP bead had better adsorption capacity, which indicated the modification by FeCl₃ enhanced adsorption ability of uranium ions.

3.7. Kinetic of uranium

One practical requirement for removal of uranium in aqueous solution is that the kinetics of reactions must be

fast. A slow reaction rate would require a prohibitively thick barrier to extend the contaminant's residence time [60,61].

Three kinetic models, including pseudo-first-order, pseudo-second-order and intra-particle diffusion models, were conducted to fit the experimental data of U(VI) adsorption on Fe-ATP. Linear mathematical expressions of these models are given in Eqs. (3)–(5):

$$\ln(q_{e1} - q_t) = \ln q_{e1} - k_1 t \quad (3)$$

$$\frac{t}{q_t} = \frac{1}{k_2 q_{e2}^2} + \frac{t}{q_{e2}} \quad (4)$$

$$q_t = k_i t^{1/2} + C \quad (5)$$

where the q_t and q_e (mg g⁻¹) are the amounts of the uranium ions adsorbed at t time (min) and equilibrium, respectively, and k_1 (min⁻¹) is the pseudo-first-order rate constant of the equation. k_2 (g mg⁻¹ min⁻¹) is the second-order rate constant. K_i (mg g⁻¹ h^{-0.5}) is the rate constant for the intraparticle transport. The C is the adsorption constant. Pseudo-first and pseudo-second order models are macroscopic kinetic models commonly used for describing adsorption process [62,63]. The resistance of intra-particle diffusion is rate-determining step. If a straight line (passing through the point of origin) is obtained, therefore, adsorption of the U(VI) ions onto the Fe-ATP bead follows a diffusion mechanism [64].

The plots of the pseudo second-order model and intra-particle diffusion kinetics model for the above equations are shown in Fig. 11 and Fig. 12, and the kinetic parameters were calculated from the linear equation as shown in Table 2. Based on the obtained correlation coefficients (R^2), the experimental data were best fitted well with the pseudo second-order model since the R^2 values for ATP bead and Fe-ATP bead were 0.9999 and 0.9957, respectively. The pseudo-first order equation for the sorption of liquid solid system based on solid capacity did not fit well (plot not shown).

According to the pseudo-second-order model, the adsorption processes could be considered as the rate-limiting step and the chemisorption involving valence forces

through the sharing or exchange of electrons between adsorbent and adsorbate could be deemed to one of the adsorption mechanisms [56,64]. The equilibrium adsorption amounts and rates could also be calculated by the mentioned models, it could be clearly seen that the equilibrium adsorption amount for ATP bead and Fe-ATP bead were 6.14 and 8.22 mg g⁻¹, respectively. The results were quite

agreement with the experimental data. There was no denying that the Fe-ATP took the advantages in immobilization of uranium from aqueous solution. More importantly, the adsorption rate for Fe-ATP bead was 0.5381 g mg⁻¹ min⁻¹, which was much greater than ATP bead. It could be concluded that the immobilization of U(VI) onto Fe-ATP bead took the both preferable capacity and adsorption rate, leading to the advantage in practical application of Fe-ATP bead for immobilization of uranium.

Considering the intra particle diffusion model, the R² for the ATP bead and Fe-ATP bead were ranged from 0.9028 to 0.9984. The adsorption of U(VI) on ATP bead and Fe-ATP also could be fitted by the intra particle diffusion model. But the lines did not pass through the point of origin from Fig. 12. In this study, the adsorption of U(VI) onto the solid adsorbents did not only follow a diffusion mechanism [64]. This deviation from the origin or near saturation might be due to the difference in the rate of mass transfer between the initial and final stages of adsorption, being consistent with pseudo-second order model. In addition, such deviation from the origin indicated that the pore diffusion was not the rate-limiting step [65]. These results indicated that intra particle diffusion and film diffusion were both the rate-limiting steps for U(VI) diffusion on the Fe-ATP bead [66,67].

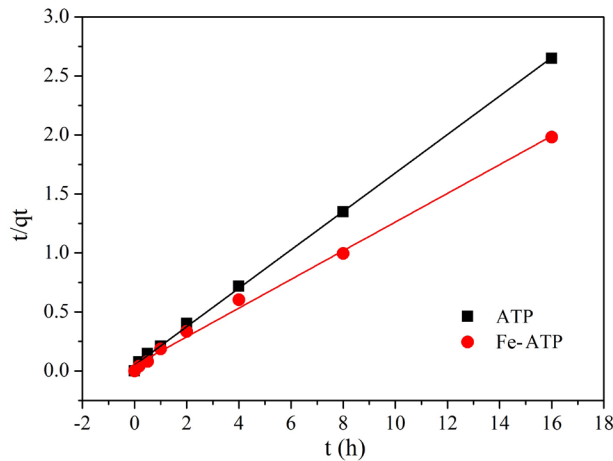


Fig. 11. Pseudo-second-order kinetic plot for the adsorption of U(VI) on ATP bead and Fe-ATP bead.

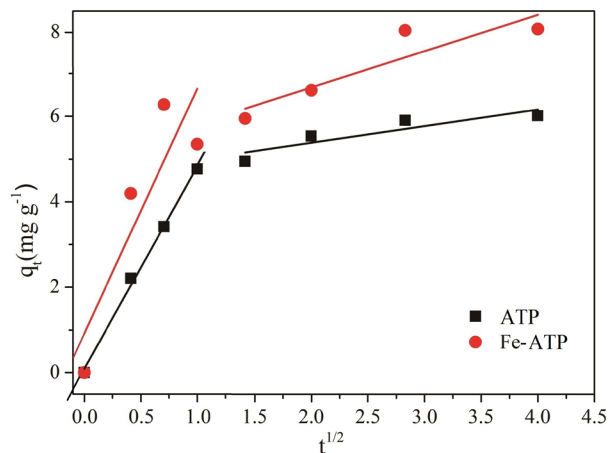


Fig. 12. Intra-particle diffusion kinetics model on adsorption of U(VI) on ATP bead and Fe-ATP bead.

3.8. Equilibrium adsorption

The initial concentration is one of the important driving forces to overcome the mass transfer resistance of U(VI) ions between the aqueous solution and solid phase. The effect of initial U(VI) concentration on adsorption was investigated at 308 K and is shown in Fig. 9. The adsorption capacity increased to 14.47 mg g⁻¹ when the initial concentration increased to 10 mg L⁻¹, while the adsorption capacity for ATP was 8.56 mg g⁻¹. The Langmuir equation and Freundlich equation [68,69] were shown in Eqs. (6) and (7) to describe the adsorption isotherms.

$$\frac{C_e}{q_e} = \frac{1}{q_0 b} + \frac{C_e}{q_0} \tag{6}$$

$$\log q_e = \log K_f + \frac{1}{n} \log C_e \tag{7}$$

where C_e is the equilibrium concentration (mg L⁻¹), q_e is the equilibrium U(VI) adsorption capacity (mg g⁻¹), q₀ is

Table 2
Parameters of kinetic model for the adsorption of U(VI) on beads

	Pseudo-first-order			Pseudo-second-order		
	q _{e1}	k (mg g ⁻¹ min ^{-1/2})	R ₁ ²	q _{e2}	k (mg g ⁻¹ min ^{-1/2})	R ₂ ²
ATP	0.3766	0.2052	0.8964	6.1402	0.3208	0.9999
Fe-ATP	0.2756	0.2523	0.7707	8.2236	0.5381	0.9957
Intra-particle diffusion						
	k _{i1} (mg g ⁻¹ min ^{-1/2})	C ₁	R ₁ ²	k _{i2} (mg g ⁻¹ min ^{-1/2})	C ₂	R ₂ ²
ATP	4.7274	0.0922	0.9984	0.3894	4.6287	0.9028
Fe-ATP	5.7258	0.9199	0.9828	0.8512	5.0042	0.9097

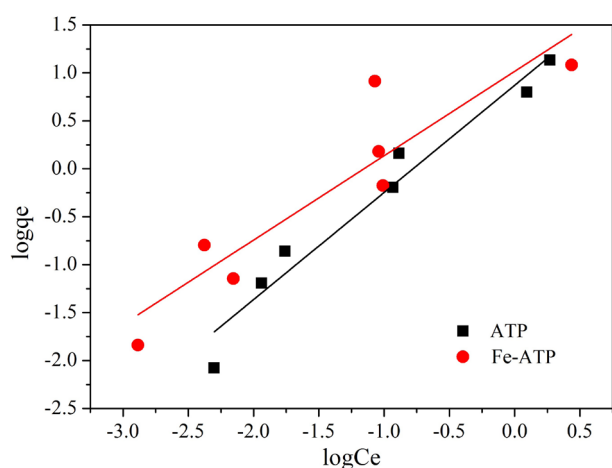


Fig.13. Freundlich isotherm of U(VI) adsorption on ATP bead and Fe-ATP bead.

Table 3

The constants and correlation coefficients for the adsorption of U(VI) on beads

	Langmuir		Freundlich			
	q_m (mg g^{-1})	b (L mg^{-1})	r_1^2	k	n	r_2^2
ATP	-1.791	-2.2952	0.9072	2.3882	1.099	0.9790
Fe-ATP	160.77	0.0846	0.6498	2.7626	1.1363	0.9135

the saturated monolayer adsorption capacity (mg g^{-1}). b is the Langmuir constant (L mg^{-1}), and relates to adsorption capacity and rate of adsorption. K_f is the Freundlich constant, relating to the adsorption capacity [$(\text{mg g}^{-1})(\text{L mg}^{-1})^{1/n}$]. n represents the adsorption intensity. The Freundlich model is suitable for the non-ideal adsorption on the heterogeneous surfaces as well as multilayer adsorption.

The detailed parameters calculated from the two models were shown in Table 3. Clearly, the Freundlich model fitted the experimental data better than Langmuir model for ATP bead and Fe-ATP bead. These results indicated that the adsorption of U(VI) onto ATP bead and Fe-ATP bead was homogeneity as well as multilayer adsorption [70]. Fe-ATP bead could be an economic adsorbent for the practical and large-scale application in immobilization of uranium.

4. Conclusion

Sodium alginate coated Fe-ATP bead were applied to remove U(VI) ions from the solutions. The result of this study showed that the adsorbent of Fe-ATP bead exhibited higher adsorption capacity compared to raw ATP. The adsorption performance of Fe-ATP bead was strongly affected by environmental conditions, such as pH, ionic strength, contact time, temperature and initial uranium concentration. The maximum capacity of the Fe-ATP bead was observed at pH 5–7. The adsorption data well fitted by

the pseudo-second order equation and Freundlich model isotherms. The adsorption of U(VI) ions onto Fe-ATP was homogeneity as well as multilayer adsorption. Taking into account the low-cost and high adsorption capacity, Fe-ATP bead could be considered as potential adsorbent for the removal of uranium from wastewater.

Acknowledgements

The authors are grateful for a research grant provided by National Natural Science Foundation of China (No. 41372233). We are grateful to the students who assisted us with this project and the anonymous reviewers of the manuscript.

References

- [1] B. Rasser, L. Desgranges, B. Pasquet, A new shielded SIMS instrument for analysis of highly radioactive materials, *Appl. Surf. Sci.*, 203 (2003) 673–678.
- [2] G.X. Zhao, T. Wen, X. Yang, S.B. Yang, J.L. Liao, J. Hu, D.D. Shao, X.K. Wang, Preconcentration of U(VI) ions on few-layered graphene oxide nano sheets from aqueous solutions, *Dalton Trans.*, 41 (2012) 6182–6188.
- [3] C. Ding, W. Cheng, Y. Sun, X. Wang, Determination of chemical affinity of graphene oxide nanosheets with radionuclides investigated by macroscopic, spectroscopic and modeling techniques, *Dalton Trans.*, 43 (2014) 3888–3896.
- [4] L. Dupont, E. Guillon, Removal of hexavalent chromium with a lignocellulosic substrate extracted from wheat bran, *Environ. Sci. Technol.*, 18 (2003) 4235–4241.
- [5] Y. Sun, Q. Wang, C. Chen, X. Tan, X. Wang, Interaction between Eu (III) and graphene oxide nanosheets investigated by batch and extended X-ray absorption fine structure spectroscopy and by modeling techniques, *Environ. Sci. Technol.*, 46 (2012) 6020–6027.
- [6] Y. Sun, D. Shao, C. Chen, S. Yang, X. Wang, Highly efficient enrichment of radionuclides on graphene oxide-supported polyaniline, *Environ. Sci. Technol.*, 47 (2013) 9904–9910.
- [7] N.J. Wang, L.L. Zhou, J. Guo, Q.Q. Ye, J.M. Lin, J.Y. Yuan, Adsorption of environmental pollutants using magnetic hybrid nanoparticles modified with beta-cyclodextrin, *Appl. Surf. Sci.*, 305 (2014) 267–273.
- [8] Y.B. Sun, Z.Y. Wu, X.X. Wang, C.C. Ding, W.C. Cheng, S.H. Yu, X.K. Wang, Macroscopic and microscopic investigation of U(VI) and Eu(III) adsorption on carbonaceous nanofibers, *Environ. Sci. Technol.*, 50 (2016) 4459–4467.
- [9] A. Ashry, E.H. Bailey, S.R.N. Chenery, S.D. Young, A kinetic study of time-dependent fixation of UVI on biochar, *J. Hazard. Mater.*, 320 (2016) 55–66.
- [10] W.C. Cheng, C.C. Ding, Y.B. Sun, X.K. Wang, Fabrication of fungus/attapulgite composites and their removal of U(VI) from aqueous solution, *Chem. Eng. J.*, 269 (2015) 1–8.
- [11] H.H. El-Maghrabi, S.M. Abdelmaged, A.A. Nada, F. Zahran, S.A. El-Wahab, D. Yahea, G.M. Hussein, M.S. Atrees, Magnetic graphene based nanocomposite for uranium scavenging, *J. Hazard. Mater.*, 322 (2017) 370–379.
- [12] Y.B. Sun, X.X. Wang, Y.J. Ai, Z.M. Yu, W. Huang, C.L. Chen, T. Hayat, A. Alsaedi, X.K. Wang, Interaction of sulfonated graphene oxide with U(VI) studied by spectroscopic analysis and theoretical calculations, *Chem. Eng. J.*, 310 (2017) 292–299.
- [13] L.Q. Tan, Y.L. Jin, X.C. Cheng, Sorption of radioeuropium onto attapulgite: effect of experimental conditions, *J. Radioanal. Nucl. Chem.*, 290 (2011) 575–585.
- [14] C. Lei, G. Xuan, Thermodynamic study of Th (VI) sorption on attapulgite, *Appl. Radi. Isotopes*, 67 (2009) 1–6.

- [15] Q.H. Fan, P. Li, Y.F. Chen, Preparation and application of attapulgite/iron oxide magnetic composites for the removal of U(VI) from aqueous solution, *J. Hazard. Mater.*, 192 (2011) 1851–1859.
- [16] A. Li, Y.G. Zhao, Study on superabsorbent composite. XII. Effect of ion-exchanged attapulgite on water absorbency of poly (acrylic acid)/attapulgite superabsorbent composites, *J. Appl. Polym. Sci.*, 105 (2007) 3476–3482.
- [17] Y.F. Zhu, Y.A. Zheng, A.Q. Wang, Preparation of granular hydrogel composite by the redox couple for efficient and fast adsorption of La(III) and Ce(III), *J. Environ. Chem. Eng.*, 3 (2015) 1416–1425.
- [18] Q.H. Fan, X.L. Tan, J.X. Li, X.K. Wang, W.S. Wu, G. Montavon, Sorption of Eu(III) on attapulgite studied by batch, XPS, and EXAFS techniques, *Environ. Sci. Technol.*, 43 (2009) 5776–5782.
- [19] C. Lei, G. Xuan, Thermodynamic study of Th (VI) sorption on attapulgite, *Appl. Radi. Isotopes*, 67 (2009) 1–6.
- [20] H. Cui, Y. Qian, Q. Li, Z.B. Wei, J.P. Zhai, Fast removal of Hg(II) ions from aqueous solution by amine-modified attapulgite, *Appl. Clay Sci.*, 72 (2013) 84–90.
- [21] Y. Liu, W.B. Wang, A.Q. Wang, Effect of dry grinding on the microstructure of palygorskite and adsorption efficiency for methylene blue, *Powder Technol.*, 225 (2012) 124–129.
- [22] Q. Liu, X. Yao, H. Cheng, R.L. Frost, An infrared spectroscopic comparison of four chinese palygorskites, *Spectrochim. Acta A*, 96 (2012) 784–789.
- [23] A.M.B.M. Oliveira, L.F.O. Coelho, S.S.S. Gomes, I.F. Costa, M.G. Fonseca, K.S. de Sousa, J.G.P. Espinola, E.C. da Silva Filho, Brazilian palygorskite as adsorbent for metal ions from aqueous solution-kinetic and equilibrium studies, *Water Air Soil Pollut.*, 224 (2013) 1–13.
- [24] W. Wang, G. Tian, Z. Zhang, A. Wang, A simple hydrothermal approach to modify palygorskite for high-efficient adsorption of methylene blue and Cu(II) ions, *Chem. Eng. J.*, 265 (2015) 228–238.
- [25] H.W. Yu, S.S. Yang, H.M. Ruan, J.N. Shen, C.J. Gao, B. Van der Bruggen, Recovery of uranium ions from simulated seawater with palygorskite/amidoxime polyacrylonitrile composite, *Appl. Clay Sci.*, 11 (2015) 67–75.
- [26] W. Zhao, P. Yuan, X.L. She, Y.Z. Xia, S. Komarneni, K. Xi, Y.K. Chen, X.D. Yao, D.J. Yang, Sustainable seaweed-based one-dimensional (1D) nanofibers as high performance electro catalysts for fuel cells, *J. Mater. Chem. A*, 3 (2015) 14188–14194.
- [27] R. Karthik, S. Meenakshi, Removal of Cr(VI) ions by adsorption onto sodium alginate-polyaniline nanofibers, *Int. J. Biol. Macromol.*, 72 (2015) 711–717.
- [28] T.Y. Kim, S.Y. Cho, S.J. Kim, Adsorption equilibrium and kinetics of copper ions and phenol onto modified adsorbents, *Adsorption*, 17(1) (2011) 135–143.
- [29] E.C. Rodrigues, B.T. Bezerra, B.V. Farias, W.S. Adriano, R.S. Vieira, D.C. Azevedo, I.J. Silva, Adsorption of cellulase isolated from *Aspergillus niger* on chitosan/alginate particles functionalized with epichlorohydrin, *Adsorpt. Sci. Technol.*, 31(1) (2013) 17–34.
- [30] N. Guo, J.S. Wang, J. Li, Y.G. Teng, Sorption study of two tetracycline antibiotics on attapulgite, *Environ. Sci. Technol.*, 38 (2015) 81–85 (In Chinese).
- [31] Y.Q. Xiang, Z.Q. Peng, D.J. Chen, A new polymer/clay nano-composite hydrogel with improved response rate and tensile mechanical properties, *Eur. Polym. J.*, 42 (2006) 2125–2132.
- [32] V.O. Arief, K. Trilestari, J. Sunarso, N. Indraswati, S. Ismadi, Recent progress on biosorption of heavy metals from liquids using low cost biosorbents: characterization, biosorption parameters and mechanism studies, *Clean-Soil Air Water*, 36 (2008) 937–962.
- [33] M.P. da Silva, M.D.F. Santos, M.R.M.C. Santos, L.D. Santos, M.G. da Fonseca, E.C. da Silva, Natural Palygorskite as an industrial dye remover in single and binary systems, *Mater. Res-Ibero-Am. J.*, 19 (2016) 1232–1240.
- [34] H. Wang, X.J. Wang, J.X. Ma, P. Xia, J.F. Zhao, Removal of cadmium (II) from aqueous solution: A comparative study of raw attapulgite clay and a reusable waste-struvite/attapulgite obtained from nutrient-rich wastewater, *J. Hazard. Mater.*, 329 (2017) 66–76.
- [35] R. Elangovan, L. Philip, K. Chandraraj, Biosorption of chromium species by aquatic weeds: Kinetics and mechanism studies, *J. Hazard. Mater.*, 152 (2008) 100–112.
- [36] I. Kiran, T. Akar, S. Tunali, Biosorption of Pb(II) and Cu(II) from aqueous solutions by pretreated biomass of *Neurospora crassa*, *Process Biochem.*, 40 (2005) 3550–3558.
- [37] L. Boudriche, R. Calvet, B. Hamdi, H. Balard, Surface properties evolution of attapulgite by IGC analysis as a function of thermal treatment, *Colloids Surf. A*, 399 (2012) 1–10.
- [38] Y. ai, J. Xue, D.A. Polya, A Fourier transform infrared spectroscopic study of Mg-rich, Mg-poor and acid leached palygorskites, *Spectrochim. Acta A*, 66 (2007) 282–288.
- [39] H. Cheng, J. Yang, R.L. Frost, Thermogravimetric analysis-mass spectrometry (TG-MS) of selected Chinese palygorskites — implications for structural water, *Thermochim. Acta*, 512 (2011) 202–207.
- [40] H. Cheng, J. Yang, R.L. Frost, Z. Wu, Infrared transmission and emission spectroscopic study of selected Chinese palygorskites, *Spectrochim. Acta A*, 83 (2011) 518–524.
- [41] M. Suárez, E. García-Romero, FTIR spectroscopic study of palygorskite: influence of the composition of the octahedral sheet, *Appl. Clay Sci.*, 31 (2006) 154–163.
- [42] C. Pang, Y.H. Liu, X.H. Cao, R. Hua, C.X. Wang, C.Q. Li, Adsorptive removal of uranium from aqueous solution using chitosan-coated attapulgite, *J. Radioanal. Nucl. Chem.*, 286 (2010) 185–193.
- [43] W.C. Cheng, C.C. Ding, Y.B. Sun, X.K. Wang, Fabrication of fungus/attapulgite composites and their removal of U(VI) from aqueous solution, *Chem. Eng. J.*, 269 (2015) 1–8.
- [44] Y. Tang, H. Zhang, X.A. Liu, D.Q. Cai, H.Y. Feng, C.G. Miao, X.Q. Wang, Z.Y. Wu, Z.L. Yu, Flocculation of harmful algal blooms by modified attapulgite and its safety evaluation, *Water Res.*, 45 (2011) 2855–2862.
- [45] Z. Zhang, W. Wang, A. Wang, Highly effective removal of Methylene Blue using functionalized attapulgite via hydrothermal process, *J. Environ. Sci.*, 33 (2015) 106–115.
- [46] K. Akhtar, A.M. Khalid, M.W. Akhtar, M.A. Ghauri, Removal and recovery of uranium from aqueous solutions by Ca-alginate immobilized *Trichoderma harzianum*, *Bioresour. Technol.*, 100 (2009) 4551–4558.
- [47] S.G. Starodoubtsev, A.A. Ryabova, A.T. Dembo, K.A. Dembo, I.I. Aliev, A.M. Wasserman, A.R. Khokhlov, Composite gels of poly(acrylamide) with interaction with cationic surfactants, ESR and SAXS study, *Macromolecules*, 35 (2002) 6362–6369.
- [48] C.L. Chen, X.K. Wang, M. Nagatsu, Europium adsorption on multiwall carbon nanotube/iron oxide magnetic composite in the presence of polyacrylic acid, *Environ. Sci. Technol.*, 43 (2009) 2362–2367.
- [49] S. Lee, P.R. Anderson, G.B. Bunker, C. Karanfil, EXAFS study of Zn sorption mechanisms on montmorillonite, *Environ. Sci. Technol.*, 38 (2004) 5426–5432.
- [50] D.L. Zhao, X.B. Wang, S.T. Yang, Z.Q. Guo, G.D. Sheng, Impact of water quality parameters on the sorption of U(VI) onto hematite, *J. Environ. Radioactiv.*, 103 (2012) 20–29.
- [51] M.L. Schlegel, M. Descostes, Uranium uptake by hectorite and montmorillonite: a solution chemistry and polarized EXAFS study, *Environ. Sci. Technol.*, 43 (2009) 8593–8598.
- [52] C. Pang, Y.H. Liu, X.H. Cao, R. Hua, C.X. Wang, C.Q. Li, Adsorptive removal of uranium from aqueous solution using chitosan-coated attapulgite, *J. Radioanal. Nucl. Chem.*, 286 (2010) 185–193.
- [53] J. Hu, D.D. Shao, C.L. Chen, G.D. Sheng, J.X. Li, X.K. Wang, M. Nagatsu, Molecular dynamics study of the structures and dynamics of the iodine molecules confined in AlPO₄-11 crystals, *J. Phys. Chem. B*, 114 (2010) 16481–16486.
- [54] C.L. Chen, J. Hu, D.D. Shao, J.X. Li, X.K. Wang, Adsorption behavior of multiwall carbon nanotube/iron oxide magnetic composites for Ni(II) and Sr(II), *J. Hazard. Mater.*, 164 (2009) 923–928.
- [55] S.S. Lu, Z.Q. Guo, C.C. Zhang, S.W. Zhang, Sorption of Th(IV) on MX-80 bentonite: effect of pH and modeling, *J. Radioanal. Nucl. Chem.*, 287 (2011) 621–628.

- [56] L.M. Zuo, S.M. Yu, H. Zhou, X. Tian, J. Jiang, Th(IV) adsorption on mesoporous molecular sieves: effects of contact time, solid content, pH, ionic strength, foreign ions and temperature, *J. Radioanal. Nucl. Chem.*, 288 (2011) 379–387.
- [57] S.W. Zhang, Z.Q. Guo, J.Z. Xu, H.H. Niu, Z.S. Chen, J.Z. Xu, Effect of environmental conditions on the sorption of radiocobalt from aqueous solution to treated eggshell as biosorbent, *J. Radioanal. Nucl. Chem.*, 288 (2011) 121–130.
- [58] C. Gok, S. Aytas, Biosorption of uranium(VI) from aqueous solution using calcium alginate beads, *J. Hazard. Mater.*, 168 (2009) 369–375.
- [59] J.S. Cao, C. Wang, F. Fang, J.X. Lin, Removal of heavy metal Cu(II) in simulated aquaculture wastewater by modified palygorskite, *Environ. Pollut.*, 219 (2016) 924–931.
- [60] Y.S. Ho, Citation review of Lagergren kinetic rate equation on adsorption reactions, *Scientometrics*, 59 (2004) 171–177.
- [61] A. Boukhelkhal, O. Benkortbi, M. Hamadache, N. Ghalem, S. Hanini, A. Amrane, Adsorptive removal of amoxicillin from wastewater using wheat grains: equilibrium, kinetic, thermodynamic studies and mass transfer, *Desal. Water Treat.*, 57 (2016) 27035–27047.
- [62] J. Choi, J.Y. Lee, J.S. Yang, Biosorption of heavy metals and uranium by starfish and *Pseudomonas putida*, *J. Hazard. Mater.*, 161 (2009) 157–162.
- [63] X.L. Jin, C. Yu, Y.F. Li, Y.X. Qi, L.Q. Yang, G.H. Zhao, H.Y. Hu, Preparation of novel nano-adsorbent based on organic–inorganic hybrid and their adsorption for heavy metals and organic pollutants presented in water environment, *J. Hazard. Mater.*, 186 (2011) 1672–1680.
- [64] J.X. Wang, C.F. Xue, Z.X. Wu, W. Li, A.M. Asiri, B. Tu, D.Y. Zhao, Hollow microporous carbon polyhedra produced by selective removal of skeletal scaffolds, *Carbon*, 50 (2012) 2546–2555.
- [65] S. Yang, P. Zong, X. Ren, Q. Wang, X. Wang, Rapid and highly efficient preconcentration of Eu(III) by core-shell structured Fe_3O_4 @humic acid magnetic nanoparticles, *ACS Appl. Mater. Interf.*, 4 (2012) 6891–6900.
- [66] A. Kamari, W.S.W. Ngah, M.Y. Chong, M.L. Cheah, Sorption of acid dyes onto GLA and H_2SO_4 cross-linked chitosan beads, *Desalination*, 249 (2009) 1180–1189.
- [67] G. Sheng, J. Hu, X. Wang, Sorption properties of Th(IV) on the raw diatomite effects of contact time, pH, ionic strength and temperature, *Appl. Radiat. Isot.*, 66 (2008) 1313–1320.
- [68] G. Sheng, J. Li, D. Shao, J. Hu, C. Chen, Y. Chen, X. Wang, Adsorption of copper(II) on multiwalled carbon nanotubes in the absence and presence of humic or fulvic acids, *J. Hazard. Mater.*, 178 (2010) 333–340.
- [69] S. Yang, D. Zhao, H. Zhang, S. Lu, L. Chen, X. Yu, Impact of environmental conditions on the sorption behavior of Pb(II) in Na-bentonite suspensions, *J. Hazard. Mater.*, 183 (2010) 632–640.
- [70] A.X. Zhou, Y.L. Zhang, R. Li, X.S. Su, L.Y. Zhang, Adsorptive removal of sulfa antibiotics from water using spent mushroom substrate, an agricultural waste, *Desal. Water Treat.*, 57 (2016) 388–397.